Core/Shell $NaGdF_4:Nd^{3+}/NaGdF_4$ Nanocrystals with Efficient Near-Infrared to Near-Infrared Downconversion Photoluminescence for Bioimaging Applications

Guanying Chen,[†,‡,⊥] Tymish Y. Ohulchanskyy,[‡] Sha Liu,[‡,§] Wing-Cheung Law,[‡] Fang Wu,[∥] Mark T. Swihart,[‡,§] Hans Ågren,[⊥] and Paras N. Prasad[‡,*]

[†]School of Chemical Engineering, Harbin Institute of Technology, 150001 Heilongjiang, People's Republic of China, [‡]Institute for Lasers, Photonics, and Biophotonics, University at Buffalo, State University of New York, Buffalo, New York 14260, United States, [⊥]Department of Theoretical Chemistry and Biology, Royal Institute of Technology, S-10691 Stockholm, Sweden, [§]Department of Chemical and Biological Engineering, University at Buffalo, State University of New York, Buffalo, New York 14260, United States, and [∥]Department of Pharmaceutical Sciences, University at Buffalo, State University of New York, Buffalo, New York 14260, United States

ABSTRACT

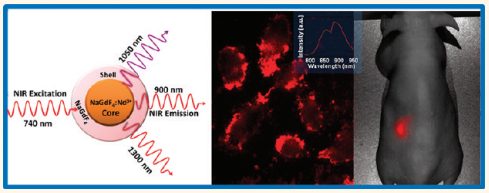

We have synthesized core/shell $NaGdF_4:Nd^{3+}/NaGdF_4$ nanocrystals with an average size of 15 nm and exceptionally high photoluminescence (PL) quantum yield. When excited at 740 nm, the nanocrystals manifest spectrally distinguished, near-infrared to near-infrared (NIR-to-NIR) downconversion PL peaked at ~900, ~1050, and ~1300 nm. The absolute quantum yield of NIR-to-NIR PL reached 40% for core–shell nanoparticles dispersed in hexane. Time-resolved PL measurements revealed that this high quantum yield was achieved through suppression of nonradiative recombination originating from surface states and cross relaxations between dopants. $NaGdF_4:Nd^{3+}/NaGdF_4$ nanocrystals, synthesized in organic media, were further converted to be water-dispersible by eliminating the capping ligand of oleic acid. NIR-to-NIR PL bioimaging was demonstrated both *in vitro* and *in vivo* through visualization of the NIR-to-NIR PL at ~900 nm under incoherent lamp light excitation. The fact that both excitation and the PL of these nanocrystals are in the biological window of optical transparency, combined with their high quantum efficiency, spectral sharpness, and photostability, makes these nanocrystals extremely promising as optical biomaging probes.

KEYWORDS: near-infrared · photoluminescence · nanocrystals · lanthanide · bioimaging

Photoluminescence (PL) imaging is an important technique used in biomedical research and, increasingly, in clinical diagnostic applications.[1,2] The development of optical probes as exogenous PL imaging contrast agents has dramatically improved the understanding of the structural and functional properties of living systems and is now impacting clinical diagnostics and therapeutics.[3−9] Ideal photoluminescent probes for *in vitro* and *in vivo* imaging would have (1) high PL quantum yield; (2) appropriate spectral range for emission/excitation wavelengths to minimize background emission and photodamage and to provide deep penetration of light in tissues; (3) good photostability; and (4) a large spectral shift between the PL emission and the excitation light to minimize excitation-light-induced background. The "optical transparency window" of biological tissues in the near-infrared (NIR) range of 700−1100 nm not only allows for deeper light penetration and reduced photodamage effects but also offers lower autofluorescence and light scattering. That, in turn, can result in a high signal-to-noise ratio (*i.e.*, high contrast) imaging.[1,10] Photoluminescent nanoparticles provide clear advantages over conventional organic fluorophores when being applied as contrast agents for optical imaging (*e.g.*, higher photostability and rich surface chemistry allowing for easy attachment of targeting bimolecules).[11] NIR-absorbing organic fluorophores are known to have relatively low quantum yield and be susceptible to photobleaching;[1] their broad PL emission spectra also limit their effectiveness in multiplexed imaging. Hence, photoluminescent nanoprobes excited by NIR light in the biological "optical transparency window" would be preferable as contrast agents for high-contrast optical imaging both *in vitro* and *in vivo*.

* Address corresponding to pnprasad@buffalo.edu.

Received for review November 2, 2011 and accepted March 8, 2012.

Published online March 08, 2012
10.1021/nn2042362

A panel of novel NIR-excitable nanomaterials has been developed for bioimaging based on their either Stokes-shifted (single-photon) or anti-Stokes-shifted (multiphoton) PL.[12−16] Quantum dots and rods (QDs and QRs) display Stokes-shifted PL under single-photon excitation conditions. They are more stable against photobleaching than organic fluorophores, and their spectrally narrow emission spectra defined by the size or aspect ratio are more suitable for multiplexed imaging.[17−19] However, NIR-emitting QDs and QRs can only be efficiently excited using visible or UV light due to the low intensity of the first excitonic absorption band.[20] Moreover, most of the NIR-emitting semiconductor materials (*e.g.*, Cd_3As_2, PbSe) were found to be less stable in comparison to those emitting in the visible range; this could significantly limit application of NIR QD-based contrast agents for bioimaging. For example, NIR-emitting Cd_3As_2 QDs are air-sensitive, with PL quantum yield declining to <1% after storage for a few days at ambient conditions.[21] The PL intensity of NIR-emitting PbSe QDs decreases significantly with an exposure to oxygen or water. Bare PbSe QDs become nearly nonluminescent after a month in air, even if stored in the dark.[22] Moreover, in addition to the chemical instability of NIR QDs (or QRs), their bioimaging applications are controversial due to the inherent toxicity of the elements they contain, such as cadmium and lead.[23] QDs and QRs are also being engaged as NIR-excitable contrast agents for anti-Stokes PL imaging through use of nonlinear two-photon excitation,[14,19] along with plasmonic nanoparticles (*e.g.*, gold nanorods, GNRs).[24] Unfortunately, just as in the case of the organic fluorophores, the cross sections of the two-photon absorption for the QDs, QRs, and GNRs are extremely low in comparison with those of the one-photon absorption; thus, the use of a high-power pulsed laser source is required to generate a detectable two-photon PL signal.[14] There are no systems currently available for whole body imaging using nonlinear two-photon excitation. Anti-Stokes PL imaging is also possible through the use of upconversion processes in lanthanide ions doped in a crystalline ceramic matrix.[15,16] These ceramic materials are generally photostable and nontoxic; they can also emit spectrally sharp and large anti-Stokes-shifted PL.[25−35] We recently demonstrated both *in vitro* and *in vivo* bioimaging employing upconverted PL from lanthanide ion-doped ceramic nanocrystals (upconversion nanophosphors).[25] Nanophosphors of NaY(Yb)F_4:Tm^{3+} were shown to be among the most promising nanomaterials for upconversion PL imaging due to exploitation of NIR-to-NIR upconversion, when both upconversion PL excitation and emission wavelengths are in the NIR "optical transparency window".[25,33] In spite of the much higher efficiency of the upconversion process when compared to the two-photon excitation,[32] the overall efficiency of the upconversion nanophosphors as PL imaging remains rather low, due to the low quantum yield of the upconversion PL. The highest quantum yield for upconversion PL reported to date is only ∼1.2% for 85 nm tetragonal $LiYF_4:Er^{3+}$ nanocrystals under 1490 nm excitation[34] and ∼0.47% for sub-10 nm hexagonal $NaLuF_4:Yb^{3+}/Tm^{3+}$ nanocrystals excited at 980 nm.[28] In addition, since multiphoton processes are involved in generation of the upconversion PL, its intensity, in general, depends nonlinearly on the excitation power density. As a result, the quantum yield of upconversion PL is usually lower at low excitation power density than that of downconversion (Stokes-shifted) PL, which does not involve multiphoton processes and can be excited with a low-power, incoherent light source. Application of the downconversion nanophosphors for bioimaging was reported by our group and others.[36−38] However, there is no prior report of NIR-to-NIR downconversion PL bioimaging *in vitro* or *in vivo* using lanthanide-doped nanocrystals under incoherent light excitation.

Among the lanthanide-doped NIR-excitable or NIR-emitting crystalline materials, Nd:YAG (Nd:$Y_3Al_5O_{12}$) is ubiquitously known as an excellent laser medium for lasing at 1064 nm due to the large absorption cross section and high quantum yield PL of Nd^{3+} ions.[39] These features would make the Nd^{3+}-containing nanocrystals promising for use in NIR PL-based bioimaging.[40,41] Although NIR PL of Nd^{3+} ions was extensively studied in several bulk crystalline matrices, reports on the Nd^{3+}-doped dispersible nanocrystals are extremely limited. Recently, van Veggel *et al.* synthesized lanthanide (Er^{3+}, Nd^{3+}, Ho^{3+})-doped colloidal LaF_3 nanocrystals for use in polymer-based optical components, because of their excellent PL in the telecommunication window of 1.3−1.5 μm.[42,43] However, these nanoparticles were not water-soluble, and the excitation was in the visible range, which limits their bioapplications. Subsequently, lanthanide-doped NdF_3 and LaF_3 nanoparticles were converted to a water-soluble form using SiO_2 coating and amphiphilic ligands.[44,45] Bednarkiewicz *et al.* reported colloidal Nd^{3+}-doped $NaYF_4$ nanoparticles, but their PL quantum yield was generally low due to nonradiative energy losses caused by the surface passivation (presence of surface impurities, interactions with ligands and solvent molecules) and by the concentration quenching effect.[46,47]

In this communication, we report on core/shell $NaGdF_4:Nd^{3+}/NaGdF_4$ nanocrystals with an average size of 15 nm, manifesting highly efficient NIR-to-NIR downconversion PL, and demonstrate the possibility of the application of the reported nanocrystals as probes for *in vitro* and *in vivo* bioimaging. The advantage offered by PL imaging with $NaGdF_4:Nd^{3+}/NaGdF_4$ nanoparticles reported here is that both the excitation wavelength of 740 nm and the PL emission at around 850−900 nm are in the biological "optical transparency

window", which is optimal for deeper tissue penetration and high contrast imaging. $NaGdF_4$ provides one of the best host lattices for lanthanide ions-doped nanoparticles because its low phonon cutoff energy can effectively reduce nonradiative losses, which in turn can increase PL quantum yield.[48,49] Moreover, the toxicity of this material is low.[50,51] In addition, $NaGdF_4$ nanoparticles have been applied as magnetic resonance imaging contrast agents, offering positive--contrast enhancement, which opens the door for multimodal imaging using Gd-containing nanoparticles.[48−54] The growth of a $NaGdF_4$ shell on $NaGdF_4$:Nd^{3+} nanoparticles suppresses nonradiative recombination processes at the nanoparticle surface,[49] which is important for producing high quantum yield PL.

RESULTS AND DISCUSSION

Synthesis of $NaGdF_4$:Nd^{3+} Nanocrystals and Core/Shell ($NaGdF_4$:Nd^{3+})/$NaGdF_4$ Nanocrystals with NIR-to-NIR Downconversion Photoluminescence. Nanocrystals of $NaGdF_4$:Nd^{3+} and ($NaGdF_4$:Nd^{3+})/$NaGdF_4$ were synthesized using the modified protocol reported elsewhere.[55] Figure 1 shows representative transmission electron microscopy (TEM) images of synthesized nanocrystals. As one can see in Figure 1A and B, the $NaGdF_4$:3% Nd^{3+} nanoparticles are nearly spherical in shape and are monodisperse, with an average diameter of about 11 nm. Figure 1D and E show that the diameter of the core/shell nanoparticle increases to about 15 nm after growth of the $NaGdF_4$ layer; the uniformity of size and shape remained almost unchanged. Histograms of the size distribution of the core and core/shell nanoparticles are shown as insets in Figure 1B and E, respectively. Figure 1C and F display the selected area electron diffraction (SAED) patterns of the core $NaGdF_4$:3% Nd^{3+} nanocrystals and the ($NaGdF_4$:3% Nd^{3+})/$NaGdF_4$ core/shell nanocrystals, respectively. The SAED patterns demonstrate that the $NaGdF_4$:3% Nd^{3+} core nanocrystals and the ($NaGdF_4$:3% Nd^{3+})/$NaGdF_4$ core/shell nanoparticles are both of hexagonal structure and can be indexed to the JCPDS 27-0699 hexagonal $NaGdF_4$ structure.

The PL spectrum of colloidal $NaGdF_4$ nanocrystals doped with 3% Nd^{3+} (hexane suspension) under laser excitation at 740 nm is shown in Figure 2A. Three PL bands are clearly resolved; they have maxima at ∼860−900, ∼1050, and ∼1330 nm, corresponding to the transitions from the $^4F_{3/2}$ state to the ^4I_J (J = 9/2, 11/2, 13/2) state of Nd^{3+} ions, respectively. The generation mechanism is based on single-photon processes, as depicted in the inset of Figure 2A. The laser at 740 nm directly excites Nd^{3+} ions from the ground $^4I_{13/2}$ state to the $^4F_{7/2}$/$^4S_{3/2}$ state; the Nd^{3+} ions at this state then decay nonradiatively to the upper-emitting $^4F_{3/2}$ state, from which radiative decays to the ^4I_J (J = 9/2, 11/2, 13/2) states generate the corresponding PL emissions. It is striking that the excitation light at 740 nm and the NIR PL bands peaked at ∼860−900 and 1050 nm are both within the "optical transparency window", which are ideal for bioimaging. Additionally, these NIR PL bands are exceptionally sharp (for example, the PL peaked at ∼1050 nm has a full width at half-maximum of only 15 nm). The Stokes shifts of all NIR PL bands are more than 100 nm; this large shift combined with sharp PL can allow high-contrast bioimaging. To check the photostability of these nanoparticles, the PL intensity was monitored as a function of the irradiation time (Figure 2B). The integrated intensity of all NIR PL bands remained unchanged for 1 h in colloidal $NaGdF_4$:3% Nd^{3+} nanocrystals, under intense laser illumination. The spectrally sharp, photostable, large Stokes-shifted, NIR-excitable PL in the NIR range suggests that $NaGdF_4$:3% Nd^{3+} nanocrystals could be very promising as bioimaging probes. Therefore, we systematically studied means of increasing the efficiency of the NIR PL in these colloidal nanocrystals.

Determination and Maximization of the Quantum Yield of NIR-to-NIR Downconversion Photoluminescence. To maximize the PL quantum yield of these nanoparticles, two steps were taken. First, the concentration of doped Nd^{3+} ions was varied to maximize the PL quantum yield; this stage aimed at minimizing the "concentration quenching effect" for the PL while maintaining a useful doping level. Second, we developed a strategy to grow a thin $NaGdF_4$ shell on the top of nanocrystals of $NaGdF_4$:Nd^{3+} optimized at the first stage. Since the size of nanocrystals of $NaGdF_4$:Nd^{3+} is only around 11 nm, a large portion of the Nd^{3+} ions are located near the particle surface; PL of these luminescent Nd^{3+} ions, therefore, is greatly quenched by surface effects (ligands, solvent, surface defects). A thin epitaxial $NaGdF_4$ shell effectively shields these Nd^{3+} ions from surface quenchers. The quantum yield of nanocrystals $NaGdF_4$:Nd^{3+} and core/shell ($NaGdF_4$:Nd^{3+})/$NaGdF_4$ was evaluated using indocynine green (DMSO solution) with a known quantum yield of 12% as a standard reference.[56] The details of the PL quantum yield measurements are presented in the Supporting Information. Figure 3A shows the absorption spectra of colloidal $NaGdF_4$ nanocrystals doped with 3, 6, 10, and 15% Nd^{3+} (hexane dispersion), ($NaGdF_4$:3% Nd^{3+})/$NaGdF_4$ core/shell nanocrystals (hexane dispersion), and indocyanine green in DMSO. As illustrated in Figure 3A, the concentrations of these samples have been adjusted to achieve matched absorbance at 740 nm, the wavelength of laser excitation. Figure 3B shows PL spectra for samples with absorption in Figure 3A. The PL intensity from nanocrystals of $NaGdF_4$:Nd^{3+} (3, 6, 10, 15%) decreases with increasing concentration of Nd^{3+}, displaying the "concentration quenching effect". The PL quantum yields for nanocrystals of $NaGdF_4$ doped with Nd^{3+} of 3, 6, 10, and 15% were estimated to be about 22, 9.4, 5.0, and 3.6%,

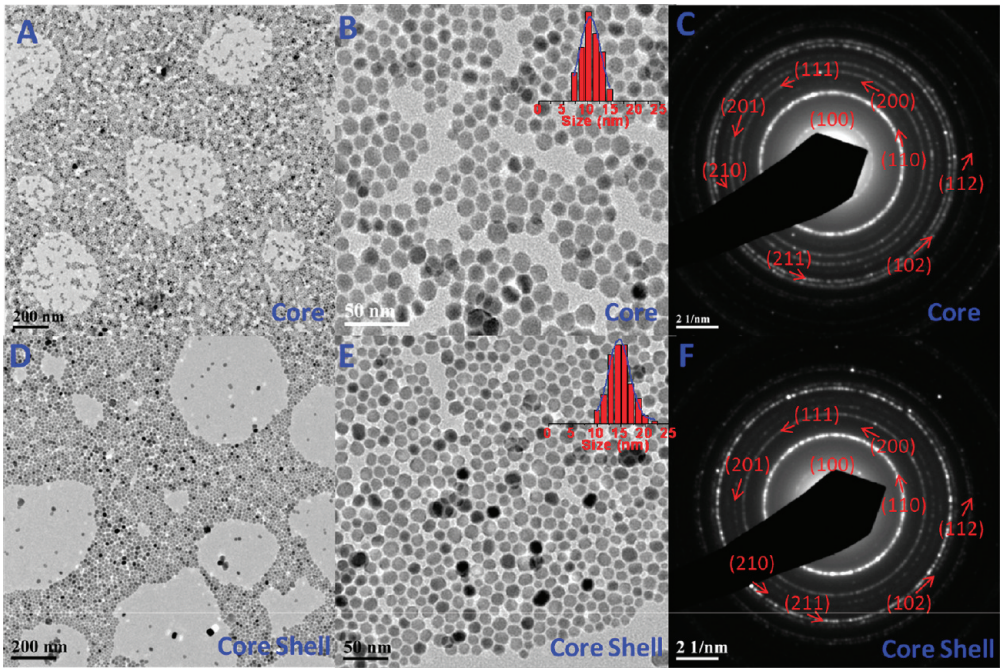

Figure 1. Transmission electron microscopy (TEM) images of $NaGdF_4$:3% Nd^{3+} (A, B) and ($NaGdF_4$:3% Nd^{3+})/$NaGdF_4$ core/shell nanocrystals (D, E) at different magnification; selected area electron diffraction patterns of the $NaGdF_4$:3% Nd^{3+} core nanocrystals (C) and ($NaGdF_4$:3% Nd^{3+})/$NaGdF_4$ core/shell nanoparticles (F). Insets in (B) and (C) display histograms of the size distribution of $NaGdF_4$:3% Nd^{3+} core and ($NaGdF_4$:3% Nd^{3+})/$NaGdF_4$ core/shell nanoparticles, respectively.

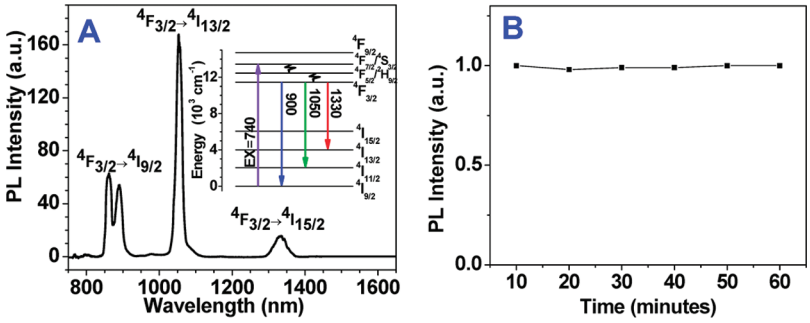

Figure 2. (A) Photoluminescence spectrum of colloidal $NaGdF_4$:3% Nd^{3+} nanocrystals under laser excitation at 740 nm (hexane suspension); (B) PL intensity of colloidal $NaGdF_4$:3% Nd^{3+} nanocrystals as a function of irradiation time by a laser at 740 nm and a power density of 0.5 W/cm^2. The inset of (A) shows the mechanism of generation of the observed PL emissions. The PL spectrum was corrected for spectral sensitivity of the spectrometer.

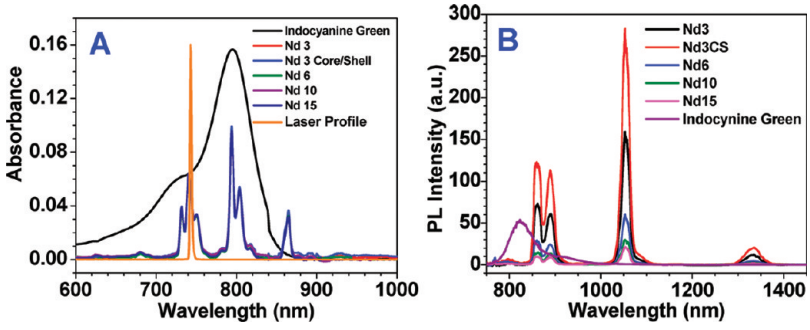

Figure 3. (A) Absorbance of colloidal $NaGdF_4$ nanocrystals doped with 3, 6, 10, and 15% Nd^{3+} (hexane dispersion), ($NaGdF_4$:3% Nd^{3+})/$NaGdF_4$ core/shell nanocrystals (hexane dispersion), and indocyanine green (DMSO solution). Absorption spectra were matched at 740 nm, corresponding to the laser excitation profile, *via* adjusting concentrations. (B) PL emissions of colloidal $NaGdF_4$ nanocrystals doped with 3, 6, 10, and 15% Nd^{3+} (hexane dispersion), ($NaGdF_4$:3% Nd^{3+})/$NaGdF_4$ core/shell nanocrystals (hexane dispersion), and indocyanine green in DMSO. The PL spectrum was corrected for spectral sensitivity of the spectrometer.

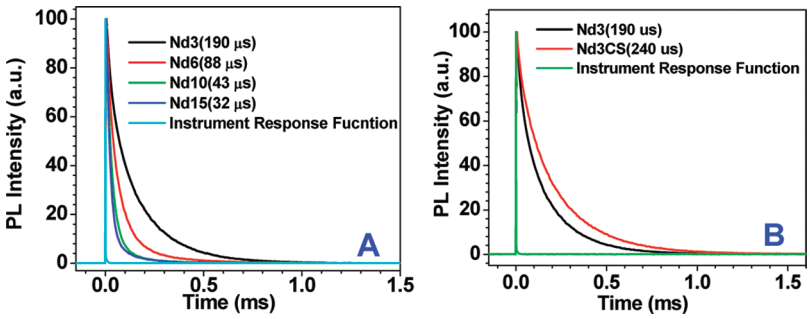

Figure 4. (A) Decays of PL emission at 860 nm in nanocrystals of $NaGdF_4$ doped with 3, 6, 10, and 15% Nd^{3+} (hexane dispersion). (B) Decays of PL emission at 860 nm in nanocrystals of $NaGdF_4$ doped with 3% Nd^{3+} and nanocrystals of core/shell ($NaGdF_4$:3% Nd^{3+})/$NaGdF_4$ (hexane dispersion).

respectively. We also prepared $NaGdF_4$ nanocrystals doped with a lower Nd^{3+} ion concentration of 1% and found that its PL intensity was about 3 times lower than that of $NaGdF_4$:Nd^{3+} 3% nanocrystals, when compared using the same molar concentration. This result suggests that the quantum yield is about the same for both samples (data not shown). Subsequently, we grew a ~2 nm thick shell of $NaGdF_4$ on the $NaGdF_4$:3% Nd^{3+} nanocrystals, in order to further increase the PL quantum yield. As displayed in Figure 3B, the PL output of the core/shell ($NaGdF_4$:Nd^{3+} 3%)/$NaGdF_4$ nanocrystals is about 1.82 times higher than that of the core $NaGdF_4$:Nd^{3+} 3% nanoparticles, meaning that the PL quantum yield is as high as 40%. Since the pure $NaGdF_4$ shell does not exhibit PL, the increased quantum yield undoubtedly originates from the effect of the shell on the core $NaGdF_4$:Nd^{3+} 3% nanocrystals. In other words, the $NaGdF_4$ shell makes the Nd^{3+} ions located on the surface of the core behave similarly to those that are within the nanocrystal matrix.

To test the "concentration quenching effect" and the "surface quenching effect", we acquired the PL decays at 860 nm of nanocrystals of $NaGdF_4$ doped with 3, 6, 10, and 15% Nd^{3+} (Figure 4A) and nanocrystals of core/shell ($NaGdF_4$:3% Nd^{3+})/$NaGdF_4$ (Figure 4B). The PL decays at other wavelengths are the same as that at 860 nm, as all NIR PL bands peaked at 900, 1050, and 1330 nm arise from the same upper energy level of the $^4F_{3/2}$ state of Nd^{3+}. As one can see in Figure 4A, the average lifetime was measured to be about 190, 88, 43, and 32 μs for nanocrystals of $NaGdF_4$ doped with Nd^{3+} of 3, 6, 10, and 15%, respectively. The shortening of lifetime with an increase in the concentration of Nd^{3+} indicates the "concentration quenching effect", agreeing well with the change of PL intensity shown in Figure 3B. It is known that the cross relaxation process of $^4F_{3/2} + {}^4I_{9/2} \rightarrow 2^4I_{15/2}$ can nonradiatively depopulate the excited $^4F_{3/2}$ level.[46] An increase in the Nd^{3+} concentration can enhance this nonradiative cross relaxation process due to closer Nd^{3+}–Nd^{3+} distance, resulting in the shortening of the lifetime of the upper-emitting $^4F_{3/2}$ level and, correspondingly, the decrease in NIR PL quantum yield. Figure 4B shows the PL decays at 860 nm for nanocrystals of $NaGdF_4$:3% Nd^{3+} and nanocrystals of core/shell ($NaGdF_4$:3% Nd^{3+})/$NaGdF_4$. A longer lifetime of 240 μs was observed for the core/shell nanocrystals in comparison with the 190 μs for core nanocrystals; the longer lifetime of PL from the core/shell system demonstrates that the shell layer isolates the emitting ions on the core surface from the quenching surface effect.

Figure 5. Photographic images of (A) oleate-capped ($NaGdF_4$:3% Nd^{3+})/$NaGdF_4$ nanocrystals dispersed in hexane and (B) ligand-free ($NaGdF_4$:3% Nd^{3+})/$NaGdF_4$ nanocrystals dispersed in water.

Optical Charactizations of Ligand-Free Water-Dispersible Core/Shell ($NaGdF_4$:3% Nd^{3+})/$NaGdF_4$ Nanocrystals. To verify whether the ($NaGdF_4$:3% Nd^{3+})/$NaGdF_4$ nanocrystals can be used for NIR-to-NIR *in vitro* and *in vivo* bioimaging, they were transferred from the organic phase to the aqueous phase by the ligand-free method using a recently reported protocol.[57] The ligand of the oleic acid in oleate-capped ($NaGdF_4$:3% Nd^{3+})/$NaGdF_4$ nanocrystals was removed through a straightforward acid treatment. Figure 5 shows photographic images of (A) oleate-capped ($NaGdF_4$:3% Nd^{3+})/$NaGdF_4$ nanocrystals dispersed in hexane and (B) ligand-free ($NaGdF_4$:3% Nd^{3+})/$NaGdF_4$ nanocrystals dispersed in water. The transparency of the ligand-free ($NaGdF_4$:3% Nd^{3+})/$NaGdF_4$ nanocrystals in water is as good as the oleate-capped nanoparticles dispersed in hexane; the colloidal suspension of the nanoparticles in water was stable, and no sedimentation was observed. The zeta potential of the ligand-free ($NaGdF_4$:3% Nd^{3+})/$NaGdF_4$ nanocrystals in water was about +30 mV (see Supporting Information Figure S1), while the hydrodynamic diameter was about 30 nm (see Supporting Information Figure S2).

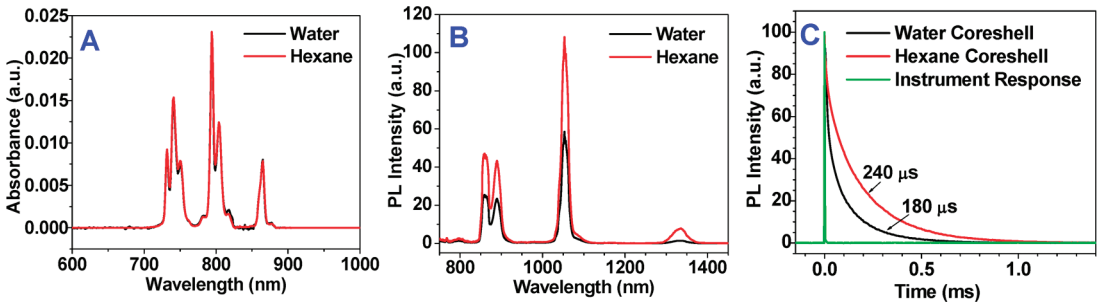

Figure 6. (A) Normalized absorbance of ($NaGdF_4$:3% Nd^{3+})/$NaGdF_4$ nanocrystals dispersed in hexane and water; (B) calibrated PL emissions of ($NaGdF_4$:3% Nd^{3+})/$NaGdF_4$ nanocrystals dispersed in hexane and water; (C) decays of PL emission at 860 nm in ($NaGdF_4$:3% Nd^{3+})/$NaGdF_4$ nanocrystals dispersed in hexane and water.

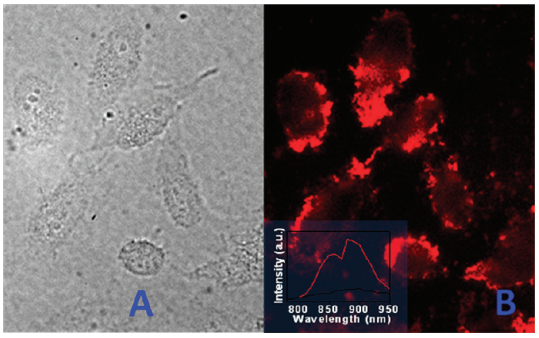

Figure 7. Transmission (A) and PL (B) images of HeLa cells treated with ligand-free ($NaGdF_4$:3% Nd^{3+})/$NaGdF_4$ nanoparticles. Inset shows localized PL spectra taken from cells (red) and background (black).

The quantum yield of ($NaGdF_4$:3% Nd^{3+})/$NaGdF_4$ nanocrystals dispersed in water was also investigated as shown in Figure 6. The intensity of PL of ($NaGdF_4$:3% Nd^{3+})/$NaGdF_4$ nanocrystals dispersed in water is about 2 times lower than that of ($NaGdF_4$:3% Nd^{3+})/$NaGdF_4$ nanocrystals dispersed in hexane (Figure 6B), meaning that the quantum yield is about 20% in water-dispersible ($NaGdF_4$:3% Nd^{3+})/$NaGdF_4$ nanocrystals. The decrease in quantum yield might arise from a multiphonon nonradiative deactivation process due to the high energy of 3350 cm^{-1} of vibrational OH. This conclusion was verified by the observation of a shorter lifetime for ($NaGdF_4$:3% Nd^{3+})/$NaGdF_4$ nanocrystals dispersed in water than for the core/shell nanocrystals dispersed in hexane (Figure 6C). On the other hand, this shortening also suggests that the shell does not provide absolute protection for Nd^{3+} ions against surface effects.

High-Contrast *in Vitro* Bioimaging Using Water-Dispersible Core/Shell ($NaGdF_4$:3% Nd^{3+})/$NaGdF_4$ Nanocrystals Under Incoherent Light Exciation. To determine whether ligand-free ($NaGdF_4$:3% Nd^{3+})/$NaGdF_4$ nanocrystals can be used for cellular imaging, we have performed *in vitro* cellular studies using HeLa cells. The cells were cultured in Dulbecco minimum essential media (MEM-R) with 10% fetal bovine serum (FBS), 1% penicillin, and 1% amphotericin B. The day before treatment, cells were seeded in 35 mm culture dishes. On treatment day, an aqueous dispersion of ligand-free ($NaGdF_4$:3% Nd^{3+})/$NaGdF_4$ was added to the cells (confluence of 50−60%), which were incubated for three hours at 37 °C. The concentration of nanoparticles in the cell medium was about 100 μg/mL, and no overt cellular toxicity was observed at a dose of 300 μg/mL (see Supporting Information Figure S3). Cellular imaging was done using a Nikon Eclipse TE 2000 microscope equipped with the Nuance GNIR CCD camera (Cambridge Research & Instrumentation Inc., CRi), which is capable of imaging in the range of 500−950 nm. An incoherent light source (halogen lamp) was used as the excitation source, in combination with a short-pass optical filter (800SP from Andover Corp). Figure 7 shows the transmission and PL images of HeLa cells treated with the ligand-free ($NaGdF_4$:3% Nd^{3+})/$NaGdF_4$ nanocrystals. The emission spectrum acquired from the cells showed the characteristic photoluminescence of Nd^{3+} in the range of ~850−900 nm (Figure 7, inset). This observation, along with a negligible background, confirms the capability of ($NaGdF_4$:3% Nd^{3+})/$NaGdF_4$ nanoparticles for high-contrast PL imaging of cells *in vitro*.

High-Contrast *in Vivo* Bioimaging Using Water-Dispersible Core/Shell ($NaGdF_4$:3% Nd^{3+})/$NaGdF_4$ Nanocrystals under Incoherent Light Exciation. To demonstrate the capability of ligand-free ($NaGdF_4$:3% Nd^{3+})/$NaGdF_4$ nanocrystals for *in vivo* bioimaging, we subcutaneously injected a nude mouse using 200 μL of 2 mg/mL nanoparticles with an injection depth of about 3 mm. The injected mouse was immediately imaged with a Maestro GNIR FLEX imaging system (CRi), using excitation light from a Xe lamp filtered with a 710−760 nm band-pass optical filter. Figure 8 presents the *in vivo* Maestro whole-body images of a nude mouse subcutaneously injected with the ligand-free ($NaGdF_4$:3% Nd^{3+})/$NaGdF_4$ nanocrystals. A clear high-contrast PL picture was observed, and the bright emission arose from the place where ($NaGdF_4$:3% Nd^{3+})/$NaGdF_4$ nanocrystals were injected (the luminescent trace of the injection needle could be distinguished); almost no autofluorescence was observed elsewhere (Figure 8B). The intense and sharp emission spectrum peaked at around 900 nm along with a weak background is shown in the inset in

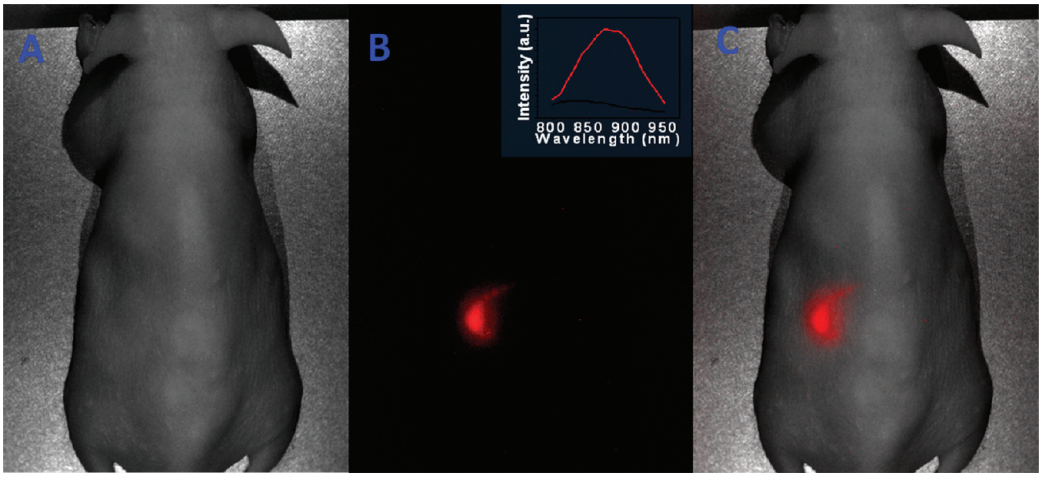

Figure 8. *In vivo* **whole-body image of a nude mouse subcutaneously injected with ligand-free ($NaGdF_4$:3% Nd^{3+})/$NaGdF_4$ nanocrystals: (a) bright field image, (b) PL image, and (c) superimposed image (bright field image and spectrally unmixed PL image). Inset in panel B is the spectra of the NIR PL signals with a background taken from the injection site and noninjected area.**

Figure 8B, illustrating the high contrast resulting from NIR-to-NIR downconversion PL imaging.

CONCLUSIONS

In conclusion, we have synthesized core/shell $NaGdF_4$:Nd^{3+}/$NaGdF_4$ nanoparticles with an average size of 15 nm, which exhibit spectrally sharp, photostable, and large Stokes-shifted NIR PL at 900, 1050, and 1300 nm when excited at 740 nm. The absolute quantum yield of this NIR-to-NIR downconversion PL was evaluated to be as high as 40% for core/shell $NaGdF_4$:Nd^{3+}/$NaGdF_4$ nanoparticles dispersed in hexane and 20% for ligand-free $NaGdF_4$:Nd^{3+}/$NaGdF_4$ nanoparticles dispersed in water. The high luminescent efficiency in nanoparticles was realized by effective suppression of nonradiative losses originating from surface passivation and cross-relaxation between Nd^{3+} dopants, as revealed by the PL steady-state and time-resolved studies. A facile high-contrast NIR-to-NIR imaging of HeLa cells and a nude mouse were demonstrated, utilizing excitation from an incoherent light source through observation of NIR PL at 900 nm.

METHODS

Synthesis of Oleate-Capped $NaGdF_4$:Nd^{3+} Core Nanocrystals. Nanocrystals of $NaGdF_4$ doped with 3, 6, 10, and 15% of Nd^{3+} ions were synthesized by a modified procedure obtained from the literature using oleic acid as coordinating ligands and 1-octadecene as noncoordinating solvent molecules.[55] All chemicals used in the synthesis were purchased from Sigma-Aldrich and used as received. In the case of $NaGdF_4$:Nd^{3+} 3% nanocrystals, 0.97 mmol of $GdCl_3 \cdot 6H_2O$ and 0.03 mmol of $NdCl_3 \cdot 6H_2O$ were mixed with 6 mL of oleic acid (90%, technical grade) and 15 mL of 1-octadecene (90%, technical grade) in a 100 mL three-neck round-bottom flask. The mixture was then heated at 160 °C for 60 min under argon flow before cooling to 50 °C. Thereafter, 10 mL of methanol solution containing 4 mmol of NH_4F and 2.5 mmol of NaOH was added quickly, and the solution was stirred at 50 °C for 30 min. After methanol was evaporated, the solution was heated to 300 °C under argon flow with vigorous stirring for 60 min. The mixture was then cooled to room temperature, precipitated by acetone in an ultrasonic bath, and collected by centrifugation at 9000 rpm for 10 min. The precipitate was washed with ethanol several times, and the nanocrystals were dispersed in 10 mL of hexane for further characterizations.

Synthesis of Oleate-Capped ($NaGdF_4$:3% Nd^{3+})/$NaGdF_4$ Core/Shell Nanocrystals. A 1 mmol amount of $GdCl_3 \cdot 6H_2O$ was added to a 100 mL three-neck round-bottom flask containing 6 mL of oleic acid (90%, technical grade) and 15 mL of 1-octadecene (90%, technical grade) and heated to 160 °C under argon gas flow with constant stirring for 60 min to form a clear solution, which was then cooled to 70 °C. Thereafter, 1 mmol of $NaGdF_4$:Nd^{3+} 3% nanocrystals in 10 mL of hexane was added to the above solution and stirred for 30 min. After the removal of hexane, 10 mL of methanol solution containing 4 mmol of NH_4F and 2.5 mmol of NaOH was then added quickly and stirred at 50 °C for 30 min. After methanol was evaporated, the solution was heated to 300 °C under argon gas flow with vigorous stirring for 60 min and then cooled to room temperature. The obtained core/shell nanoparticles were precipitated by addition of acetone, collected by centrifugation at 9000 rpm for 10 min, washed with ethanol several times, and finally dispersed in 10 mL of hexane.

Transferring ($NaGdF_4$:3% Nd^{3+})/$NaGdF_4$ Core/Shell Nanocrystals from Hexane Solution to Aqueous. Oleate-capped ($NaGdF_4$:3% Nd^{3+})/$NaGdF_4$ core/shell nanocrystals in hexane were transferred into the aqueous phase through a modified ligand-free protocol.[57] Typically, ($NaGdF_4$:3% Nd^{3+})/$NaGdF_4$ core/shell nanocrystals dispersed in 10 mL of hexane were dried in a 20 mL vial under gentle air gas flow. Deionized water (10 mL) was then added into the vial; its pH value was decreased to 2−4 using 0.1 M HCl. The mixture of powders and water was sonicated for about 4 h while maintaining the pH value of 2−4 by adding 0.1 M HCl every 30 min. The carboxylate groups of the oleate ligand were gradually protonated to yield oleic acid. After completion of this process, the aqueous solution was mixed with diethyl ether to remove the oleic acid by extraction. The procedure was repeated several times until the solution become totally transparent. The ligand-free ($NaGdF_4$:3% Nd^{3+})/$NaGdF_4$ core/shell nanocrystals in water were recovered by centrifugation at 9000 rpm for 10 min after precipitation with acetone. The product was then redispersed in acetone, centrifuged, and finally dispersed in deionized water.

Characterizations of $NaGdF_4$:Nd^{3+} Nanocrystals and ($NaGdF_4$:3% Nd^{3+})/$NaGdF_4$ Core/Shell Nanocrystals. The size and morphology of the nanocrystals were characterized by transmission electron microscopy using a JEM-2010 microscope at an acceleration voltage of 200 kV. Near-infrared photoluminescence spectra were recorded using a SPEX 270 M spectrometer (Jobin Yvon) equipped with an InGaAs TE-cooled photodiode (Electro-Optical Systems, Inc.). The PL spectra were corrected for the spectral sensitivity of the spectral system using as a reference the blackbody emission of a tungsten bulb with a color temperature of about 2900 K.[58] Laser excitation of 740 nm was provided by a tunable Ti:Sapphire laser (Tsunami from Spectra Physics) operating in free-running (unlocked) mode. The PL signal of the sample in the cuvette was collected at 90° relative to the excitation light. Absorption spectra of colloidal nanocrystal suspensions and indocynine green solution were acquired using a Shimadzu 3600 UV−visible−NIR scanning spectrophotometer. The PL decays at 860 nm were acquired using an Infinium oscilloscope (Hewlett-Packard) coupled to the PMT of a Fluorolog-3.11 Jobin Yvon spectrofluorometer. Excitation at 532 nm from a nanosecond pulsed Nd:YAG laser (Lotis TII, Belarus) at a repetition rate of 20 Hz was used for PL excitation in the decay study. Photographic images of colloidal nanocrystals were taken by a digital camera (Lumix DMC-Fx520, Japan) without any filter or image processing. The zeta potential and hydrodynamic size of ligand-free ($NaGdF_4$:3% Nd^{3+})/$NaGdF_4$ nanocrystals were measured by a 90 Plus/particle size analyzer (Brookhaven Instruments Corporation).

***In Vivo* Imaging Using ($NaGdF_4$:3% Nd^{3+})/$NaGdF_4$ Core/Shell Nanocrystals.** Multispectral (wavelength-resolved) *in vivo* imaging was carried out using a Maestro GNIR Flex imaging system (CRi) along with image acquisition and analysis software from CRi. When the tunable liquid crystal filter in the Nuance GNIR CCD camera (Cambridge Research & Instrumentation Inc., CRi) was stepped by an increment of 10 nm from 800 to 950 nm, the whole-body image of a nude mouse was captured with a constant exposure time at each step. The acquisition time was about 10 s for the whole spectral range. The NIR excitation was performed using the Xe lamp of the CRi system with the passing defined by a 710−760 band-pass filter, while a 800 nm long-pass filter was used and put in front of the Nuance GNIR CCD camera for imaging. The resulting TIF image at each step was packed into a database in memory with every pixel having its own spectrum. Therefore, small but meaningful spectral differences could be rapidly detected and analyzed using the CRi spectral imaging software. The background spectra and the NIR PL spectra from the ($NaGdF_4$:3% Nd^{3+})/$NaGdF_4$ were manually selected from the spectral image using the computer mouse to choose appropriate regions. Spectral unmixing algorithms (available from CRi) were applied to create the unmixed background image and NIR PL image. After the generation of unmixed images, the background image should be uniform in intensity in the entire imaging area. The spectra of background and NIR PL used for the unmixing process were then saved in the spectral libraries and output and shown in the inset of Figure 8B.

Conflict of Interest: The authors declare no competing financial interest.

Acknowledgment. This work was supported by grants from the National Institutes of Health (R01CA119358 and RO1CA104492), the Swedish Energy Agency (project 32076-1), and the John R. Oishei Foundation.

Supporting Information Available: Details of measurements of the zeta potential, cellular toxicity assessment, hydrodynamic dynameter of ($NaGdF_4$:3% Nd^{3+})/$NaGdF_4$ core/shell nanocrystals, and PL quantum yield. This material is available free of charge *via* the Internet at http://pubs.acs.org.

REFERENCES AND NOTES

1. Prasad, P. N. *Introduction to Biophotonics*; Wiley-Interscience: New York, 2004; pp 203−310.
2. Prasad, P. N. *Nanophotonics*; Wiley-Interscience: New York, 2004; pp 355−388.
3. Bruchez, M., Jr.; Moronne, M.; Gin, P.; Weiss, S.; Alivisatos, A. P. Semiconductor Nanocrystals as Fluorescent Biological Labels. *Science* **1998**, *281*, 2013–2016.
4. Chan, W. C. W.; Nie, S. Quantum Dot Bioconjugates for Ultrasensitive Nonisotopic Detection. *Science* **1998**, *281*, 2016–2018.
5. Weissleder, R. A Clearer Vision for *In Vivo* Imaging. *Nat. Biotechnol.* **2001**, *19*, 316–317.
6. Yang, R. H.; Jin, J. Y.; Chen, Y.; Shao, N.; Kang, H. Z.; Xiao, Z. Y.; Tang, Z. W.; Wu, Y. R.; Zhu, Z.; Tan, W. H. Carbon Nanotube-Quenched Fluorescent Oligonucleotides: Probes that Fluoresce upon Hybridization. *J. Am. Chem. Soc.* **2008**, *130*, 8351–8358.
7. Ow, H.; Larson, D. R.; Srivastava, M.; Baird, B. A.; Webb, W. W.; Wiesner, U. Bright and Stable Core-Shell Fluorescent Silica Nanoparticles. *Nano Lett.* **2005**, *5*, 113–117.
8. Welsher, K.; Liu, Z.; Sherlock, S.; Robinson, J.; Chen, Z.; Daranciang, D.; Dai, H. J. A Route to Brightly Fluorescent Carbon Nanotubes for Near-Infrared Imaging in Mice. *Nat. Nanotechnol.* **2009**, *4*, 773–780.
9. Park, J.; Gu, L.; Maltzahn, G.; Ruoslahti, E.; Bhatia, S. N.; Sailor, M. J. Biodegradable Luminescent Porous Silicon Nanoparticles for *In Vivo* Applications. *Nat. Mater.* **2009**, *8*, 331–336.
10. Smith, A. M.; Mancini, M. C.; Nie, S. M. Second Window for *In Vivo* Imaging. *Nat. Nanotechnol.* **2009**, *4*, 710–711.
11. Resch-Genger, U.; Ute, Grabolle, M.; Cavaliere-Jaricot, S.; Nitschke, R.; Nann, T. Quantum Dots *versus* Organic Dyes as Fluorescent Labels. *Nat. Methods* **2008**, *5*, 763–775.
12. Hilderbrand, S.; Weissleder, R. Near-Infrared Fluorescence: Application to *In Vivo* Molecular Imaging. *Curr. Opin. Chem. Biol.* **2010**, *14*, 71–79.
13. Sharma, P.; Brown, S.; Walter, G.; Santra, S.; Moudgil, B. Nanoparticles for Bioimaging. *Adv. Colloid Interface Sci.* **2006**, *123−126*, 471–485.
14. Ohulchanskyy, T. Y.; Roy, I.; Yong, K. T.; Pudavar, H. E.; Prasad, P. N. High-Resolution Light Microscopy Using Luminescent Nanoparticles. *Nanomed. Nanobiotechnol.* **2010**, *2*, 162–175.
15. Wang, F.; Banerjee, D.; Liu, Y. S.; Chen, X. Y.; Liu, X. G. Upconversion Nanoparticles in Biological Labeling, Imaging, and Therapy. *Analyst* **2010**, *135*, 1839–1854.
16. Mader, H.; Kele, P.; Saleh, S.; Wolfbeis, O. Upconverting Luminescent Nanoparticles for Use in Bioconjugation and Bioimaging. *Curr. Opin. Chem. Biol.* **2010**, *14*, 582–596.
17. Alivisatos, A. The Use of Nanocrystals in Biological Detection. *Nat. Biotechnol.* **2004**, *22*, 47–52.
18. Ruan, G.; Agrawal, A.; Marcus, A. I.; Nie, S. Imaging and Tracking of Tat Peptide-Conjugated Quantum Dots in Living Cells: New Insights into Nanoparticle Uptake, Intracellular Transport, and Vesicle Shedding. *J. Am. Chem. Soc.* **2007**, *129*, 14759–14766.
19. Yong, K.-T.; Qian, J.; Roy, I.; Lee, H. H.; Bergey, E. J.; Tramposch, K. M.; He, S.; Swihart, M. T.; Maitra, A.; Prasad, P. N. Quantum Rod Bioconjugates as Targeted Probes for Confocal and Two-Photon Fluorescence Imaging of Cancer Cells. *Nano Lett.* **2007**, *7*, 761–765.
20. Gao, J. H.; Chen, K.; Xie, R. G.; Xie, J.; Lee, S.; Cheng, Z.; Peng, X. G.; Chen, X. Y. Ultrasamll Near-Infrared Non-Cadmium Quantum Dots for *In Vivo* Tumor Imaging. *Small* **2010**, *6*, 256–261.
21. Harris, D. K.; Allen, P. M.; Han, H. S.; Walker, B. J.; Lee, J. M.; Bawendi, M. G. Synthesis of Cadmium Arsenide Quantum Dots Luminescent in the Infrared. *J. Am. Chem. Soc.* **2011**, *133*, 4676–4679.
22. Stouwdam, J.; Shan, J. N.; Veggel, F.; Pattantyus-Abraham, A. G.; Youg, J. F. Photostability of Colloidal PbSe and PbSe/PbS Core/Shell Nanocrystals in Solution and in the Solid State. *J. Phys. Chem. C* **2007**, *111*, 1086–1092.
23. Hardman, R. A Toxicologic Review of Quantum Dots: Toxicity Depends on Physicochemical and Environmental Factors. *Environ. Health Perspect.* **2006**, *114*, 165–172.
24. Durr, N. J.; Larson, T.; Smith, D. K.; Korgel, B. A.; Sokolov, K.; Ben-Yakar, A. Two-Photon Luminescence Imaging of Cancer Cells Using Molecularly Targeted Gold Nanorods. *Nano Lett.* **2007**, *7*, 941–545.

25. Nyk, M.; Kumar, R.; Ohulchanskyy, T. Y.; Bergey, E. J.; Prasad, P. N. High Contrast *In Vitro* and *In Vivo* Photoluminescence Bioimaging Using Near Infrared to Near Infrared Up-Conversion in Tm^{3+} and Yb^{3+} Doped Fluoide Nanophosphors. *Nano Lett.* **2008**, *8*, 3834–3838.
26. Chatterjee, D. K.; Rufaihah, A. J.; Zhang, Y. Upconversion Fluorescence Imaging of Cells and Small Animals Using Lanthanide Doped Nanocrystals. *Biomaterials* **2008**, *29*, 937–943.
27. Liu, Q.; Sun, Y.; Li, C. G.; Zhou, J.; Li, C. Y.; Yang, T. S.; Zhang, X. Z.; Yi, T.; Wu, D. M.; Li, F. Y. ^{18}F-Labeled Magnetic-Upconversion Nanophosphors *via* Rare-Earth Cation-Assisted Ligand Assembly. *ACS Nano* **2011**, *5*, 3146–3157.
28. Liu, Q.; Sun, Y.; Yang, T. S.; Feng, W.; Li, C. G.; Li, F. Y. Sub-10 nm Hexagonal Lanthanide-Doped $NaLuF_4$ Upconversion Nanocrystals for Sensitive Bioimaging *In Vivo*. *J. Am. Chem. Soc.* **2011**, *133*, 17122–17125.
29. Xong, L. Q.; Yang, T. S.; Yang, Y.; Xu, C. J.; Li, F. Y. Long-Term *In Vivo* Biodistribution Imaging and Toxicity of Polyacrylic Acid-Coated Upconversion Nanophosphors. *Biomaterials* **2010**, *31*, 7078–7085.
30. Cheng, L.; Yang, K.; Zhang, S.; Shao, M. W.; Lee, S. T.; Liu, Z. Highly-Sensitive Multiplexed *In Vivo* Imaging Using PEGylated Upconversion Nanoparticles. *Nano Res.* **2010**, *3*, 722–732.
31. Yi, G. S.; Lu, H. C.; Zhao, S. Y.; Ge, Y.; Yang, W. J.; Chen, D. P.; Guo, L. H. Synthesis, Characterization, and Biological Application of Size-Controlled Nanocrystalline $NaYF_4$:Yb,Er Infrared-to-Visible Up-Conversion Phosphors. *Nano Lett.* **2004**, *4*, 2191–2196.
32. Haase, M.; Schäfer, H. Upconverting Nanoparticles. *Angew. Chem., Int. Ed.* **2011**, *50*, 5808–5829.
33. Chen, G. Y.; Ohulchanskyy, T. Y.; Kumar, R.; Ågren, H.; Prasad, P. N. Ultrasmall Monodisperse $NaYF_4$:Yb^{3+}/Tm^{3+} Nanocrystals with Enhanced Near-Infrared to Near-Infrared Upconversion Photoluminescence. *ACS Nano* **2010**, *4*, 3163–3168.
34. Chen, G. Y.; Ohulchanskyy, T. Y.; Kachynski, A.; Ågren, H.; Prasad, P. N. Intense Visible and Near-Infrared Upconversion Photoluminescence in Colloidal $LiYF_4$:Er^{3+} Nanocrystals under Exciation at 1490 nm. *ACS Nano* **2011**, *5*, 4981–4986.
35. Boyer, J.; Veggel, F. Absolute Quantum Yield Measurements of Colloidal $NaYF_4$:Er^{3+},Yb^{3+} Upconverting Nanocrystals. *Nanoscale* **2010**, *2*, 1417–1419.
36. Kumar, R.; Nyk, M.; Ohulchanskyy, T. Y.; Bergey, E. J.; Prasad, P. N. Combined Optical and MR Bioimaging Using Rare Earth Ion Doped $NaYF_4$ Nanocrystals. *Adv. Funct. Mater.* **2009**, *19*, 853–859.
37. Shen, J.; Sun, L. D.; Zhu, J. D.; Wei, L. H.; Sun, H. F.; Yan, C. H. Biocompatible Bright YVO_4:Eu Nanoparticles as Versatile Optical Bioprobes. *Adv. Funct. Mater.* **2010**, *20*, 3708–3714.
38. Sun, C.; Carpenter, C.; Pratx, G.; Xing, L. Facile Synthesis of Amine-Functionalized Eu^{3+}-Doped $La(OH)_3$ Nanophosphors for Bioimaging. *Nanoscale Res. Lett.* **2011**, *6*, 24.
39. Singh, S.; Smith, R. G.; Uitert, L. G. Stimulated-Emission Cross Section and Fluorescent Quantum Efficiency of Nd^{3+} in Yttrium Aluminum Garnet at Room Temperature. *Phys. Rev. B* **1974**, *10*, 2566–2572.
40. Bünzli, J. C. G. Lanthanide Luminescence for Biomedical Analyses and Imaging. *Chem. Rev.* **2010**, *110*, 2729–2755.
41. Zhang, J.; Shade, C. M.; Chengelis, D. A.; Petoud, S. A Strategy to Protect and Sensitize Near-Infrared Luminescent Nd^{3+} and Yb^{3+}: Organic Tropolonate Ligands for the Sensitization of Ln^{3+}-Doped $NaYF_4$ Nanocrystals. *J. Am. Chem. Soc.* **2007**, *129*, 14834–14835.
42. Stouwdam, J. W.; Veggel, F. C. J. M. Near-Infrared Emission of Redispersible Er^{3+}, Nd^{3+}, and Ho^{3+} Doped LaF_3 Nanoparticles. *Nano Lett.* **2002**, *2*, 733–737.
43. Hebbink, G. A.; Stouwdam, J. W.; Reinhoudt, D. N.; Veggel, F. C. J. M. Lanthanide(III)-Doped Nanoparticles That Emit in the Near-Infrared. *Adv. Mater.* **2002**, *14*, 1147–1150.
44. Wang, F.; Zhang, Y.; Fan, X. P.; Wang, M. Q. Facile Synthesis of Water-Soluble LaF_3:Ln^{3+} Nanocrystals. *J. Mater. Chem.* **2006**, *16*, 1031–1034.
45. Yu, X. F.; Chen, L. D.; Li, M.; Xie, M. Y.; Zhou, L.; Li, Y.; Wang, Q. Q. Highly Efficient Fluorescence of NdF_3/SiO_2 Core/Shell Nanoparticles and the Applications for *In Vivo* NIR Detection. *Adv. Mater.* **2008**, *20*, 4118–4123.
46. Bednarkiewicz, A.; Wawrzynczyk, D.; Nyk, M.; Strek, W. Synthesis and Spectral Properties of Colloidal Nd^{3+} Doped $NaYF_4$ Nanocrystals. *Opt. Mater.* **2011**, *33*, 1481–1486.
47. Bednarkiewicz, A.; Wawrzynczyk, D.; Nyk, M.; Strek, W. Optically Stimulated Heating Using Nd^{3+} Doped $NaYF_4$ Colloidal Near Infrared Nanophosphors. *Appl. Phys. B: Laser Opt.* **2011**, *103*, 847–852.
48. Liu, Y. S.; Tu, D. T.; Zhu, H. M.; Li, R. F.; Luo, W. T.; Chen, X. Y. A Strategy to Achieve Efficient Dual-Mode Luminescence of Eu^{3+} in Lanthanides Doped Multifuncitonal $NaGdF_4$ Nanocrystals. *Adv. Mater.* **2010**, *22*, 3266–3271.
49. Wang, F.; Wang, J.; Liu, X. G. Direct Evidence of a Surface Quenching Effect on Size-Dependent Luminescence of Upconversion Nanoparticles. *Angew. Chem., Int. Ed.* **2010**, *49*, 7456–7460.
50. Zhou, J.; Sun, Y.; Du, X. X.; Xiong, L. Q.; Hu, H.; Li, F. Y. Dual-Modality *In Vivo* Imaging Using Rare-Earth Nanocrystals with Near-Infrared to Near-Infrared (NIR-to-NIR) Upconversion Luminescence and Magnetic Resonance Properties. *Biomaterials* **2010**, *31*, 3287–3295.
51. Zhou, J.; Liu, Z.; Li, F. Y. Upconversion Nanophosphors for Small-Animal Imaging. *Chem. Soc. Rev.* **2012**, *41*, 1323–1349.
52. Park, Y.; Kim, J. H.; Lee, K. T.; Jeon, K. S.; Na, H. B.; Yu, J. H; Kim, H. M.; Lee, N.; Choi, S. H.; Baik, S.; *et al.* Nonblinking and Nonbleaching Upconverting Nanoparticles as an Optical Imaging Nanoprobe and T1 magnetic Resonance Imaging Contrast Agent. *Adv. Mater.* **2009**, *21*, 4467–4471.
53. Chen, G. Y.; Ohulchanskyy, T. Y.; Law., W. C.; Ågren, H.; Prasad, P. N. Monodisperse $NaYbF_4$:Tm^{3+}/$NaGdF_4$ Core/Shell Nanocrystals with Near-Infrared to Near-Infrared Upconversion Photoluminescence and Magnetic Resonance Properties. *Nanoscale* **2011**, *3*, 2003–2008.
54. Johnson, N. J. J.; Oakden, W.; Stanisz, G. J.; Prosser, R. S.; Veggel, F. C. J. M. Size-Tunable, Ultrasmall $NaGdF_4$ Nanoparticles: Insights into Their T1MRI Contrast Enhancement. *Chem. Mater.* **2011**, *23*, 3714–3722.
55. Qian, H.; Zhang, Y. Synthesis of Hexagonal-Phase Core-Shell $NaYF_4$ Nanocrystals with Tunable Upconversion Fluorescence. *Langmuir* **2008**, *24*, 12123–12125.
56. Bension, R. C.; Kues, H. A. Fluorescence Properties of Indocyanine Green as Related to Angiography. *Phys. Med. Biol.* **1978**, *23*, 159–163.
57. Bogdan, N.; Vetrone, F.; Ozin, G. A.; Capobianco, J. A. Synthesis of Ligand-Free Colloidally Stable Water Dispersible Brightly Luminescent Lanthanide-Doped Upconverting Nanoparticles. *Nano Lett.* **2011**, *11*, 835–840.
58. Svanberg, S. *Atomic and Molecular Spectroscopy: Basic Aspects and Practical Applications*; Springer-Verlag: New York, 2004; pp 106−107.